Near-fault earthquakes with pulse-like horizontal and vertical seismic ground motion components: analysis and effects on elastomeric bearings

Giuseppe Quaranta[a], Giulia Angelucci[b], Fabrizio Mollaioli[b]

[a]*Department of Structural and Geotechnical Engineering, Sapienza University of Rome, Via Eudossiana 18, 00184 Rome, Italy*

[b]*Department of Structural and Geotechnical Engineering, Sapienza University of Rome, Via Gramsci 53, 00197 Roma, Italy*

Abstract

Near-fault earthquakes have been largely studied in the last years by paying special attention to the occurrence of a pulse-like horizontal seismic ground motion, and to the related effects on structural systems. Conversely, less attention has been paid on the vertical component of the ground motion in such seismic events. Within this framework, the present study is meant at investigating a fairly overlooked special case, that is the occurrence of near-fault earthquakes exhibiting a pulse-like seismic ground motion along the horizontal direction and the vertical one. Specifically, the variational mode decomposition technique is employed to prepare and characterize two subsets of near-fault earthquake records that consist of fault-normal and vertical seismic ground motion components. One subset collects earthquake records with pulse-like waveform in both velocity components, whereas a pulse-like waveform in the fault-normal velocity component only takes place in the earthquake records of the second subset. If both fault-normal and vertical components embed a dominant pulse-like waveform, then it is found that the ratio of the corresponding pulse periods well correlates with the pulse period along the fault-normal direction, while it is uncorrelated with respect to the pulse period along the vertical direction. Next, it is investigated the displacement demand of high-damping rubber bearings for base-isolated buildings under earthquake records characterized by a horizontal impulsive ground motion together with either a pulse-like or a nonpulse-like vertical shaking, provided that the pulse period in the horizontal direction is similar and the peak ground accelerations are individually the same after scaling. Final results shows that the maximum displacement of elastomeric bearings subjected to a pulse-like horizontal ground motion is moderately amplified, on average, when the vertical excitation is also pulse-like.

Keywords: Base isolation, High-damping rubber bearing, Near-fault earthquake, Pulse-like seismic ground motion, Vertical seismic ground motion.

1. Introduction

Nowadays, the awareness of the higher seismic risk to which built environment can be exposed because of the impulsive characteristic of the ground motion near the causative fault is well-established. This is

the result of the significant efforts made so far in order to achieve a more complete understanding of such dynamic loading condition as well as of its effects on structural systems.

In this sense, Ertuncay and Costa [15] have found that fault type, moment magnitude, distance and azimuth between a site of interest and the surface projection of the ruptured fault are correlated with the impulsiveness of the seismic events. A significant number of recent studies have also focused on how the dominant pulse can be identified in the seismic ground motion. Among the alternative methods proposed for processing pulse-like seismic ground motion records, some of them rely on a time-frequency decomposition, such as the wavelet decomposition-based approach illustrated by Baker [3], the empirical mode decomposition implemented by Xu and Agrawal [61], the modified S-transform proposed by Amiri and Moghaddam [2], and the variational mode decomposition employed by Quaranta and Mollaioli [51]. An energy-based standpoint is often adopted to evaluate the seismic demand due to earthquakes that causes a pulse-like shaking [10], and the time-frequency analysis was proven very useful to characterize their damage potential [47, 64]. Furthermore, parametric analytical models have been presented over the years to simulate pulse-like seismic waveforms as well, for instance, by Menun and Fu [43] and Mavroeidis and Papageorgiou [37]. Probabilistic predictive relationships have been proposed by Halldórsson et al. [24] as well as Dabaghi and Der Kiureghian [6] for the parameters of the numerical waveform proposed by Mavroeidis and Papageorgiou [37].

Parallel to that, several studies have investigated to what extent the performance of structural systems is affected by pulse-like seismic ground motions, essentially considering the horizontal shaking only. Alavi and Krawinkler [1] were among the first ones that provided a general description of the effects of a horizontal pulse-like seismic ground motion on the inelastic response of frame structures. They found that early yielding occurs in the higher stories of structures with a period longer than the pulse period, but the high ductility demands migrate to the bottom stories as the severity of the ground motion increases. Conversely, the maximum demand always occurs in the bottom stories of the structures with a period shorter than the pulse period. Specific conclusions about steel and reinforced concrete frames [7, 11, 18, 32, 35, 58, 63] agree on the fact that higher seismic demand levels often occur under pulse-like ground motions as compared to those observed under nonpulse-like ground motions. Several studies have also devoted to assess or improve the performance of structural systems under horizontal pulse-like seismic ground motion when they are equipped with protection devices, such as tuned mass dampers [36, 53, 57], viscous or hysterestic dampers [12, 20, 34, 49, 62], and isolation bearings [4, 21–23, 26, 48, 50, 55, 56, 59]. Recently, Dao et al. [8] have developed practical formulations to predict the peak displacement of isolation bearings from equivalent linear force procedures under the hypotheses of rigid superstructure and bilinear behavior of the isolators. Their statistical analysis highlighted that the displacement demand of the isolators depends on the nature of the seismic ground motion (i.e. far-field, nonpulse-like near-field, or pulse-like near-field), but final results take into account the role of the horizontal component only.

Indeed, following a common trend in seismic design, there are far fewer studies about the vertical shaking

in near-fault earthquakes. In this regard, Ertuncay and Costa [15], among the others, pointed out recently that some of the earthquake records with impulsive seismic signals in the horizontal direction also exhibit vertical pulses. A statistical investigation about the features of pulse- and nonpulse-like vertical ground motion records in near-fault earthquakes has been also presented recently by Khansefid [28] for the Iranian Plateau. On the other hand, Mazza and his co-authors have provided useful results about the performance of base-isolated frames equipped with elastomeric bearings under near-fault earthquakes considering, both, horizontal and vertical shaking [38, 40, 42]. However, it is not know yet whether the specific waveform of the vertical seismic ground motion (i.e., pulse- or nonpulse-like) has some influence on the response of elastomeric bearings or not. Besides a further insight about the characteristics of the vertical component in near-fault earthquakes, this is an issue that the present work aims at dealing with.

This paper is thus concerned with near-fault earthquakes exhibiting a pulse-like seismic ground motion along a horizontal direction and the vertical one. In this perspective, the original contributions of the present work are twofold. First, it is shown that, if both horizontal fault-normal and vertical components embed a dominant pulse-like waveform, then the ratio of the corresponding pulse periods well correlates with the pulse period along the fault-normal direction, while it is uncorrelated with respect to the pulse period along the vertical direction. Moreover, a statistical study is performed in order to examine the effect of the vertical seismic ground motion on the maximum displacement of high-damping rubber bearings for base-isolated buildings, in such a way to understand whether the fact that it may be or not pulse-like does matter. Final results demonstrates that the maximum displacement of elastomeric bearings subjected to a pulse-like horizontal fault-normal ground motion can increase moderately, on average, if the vertical excitation is also pulse-like.

2. Analysis of pulse-like seismic ground motion records

Quaranta and Mollaioli [51] proposed the application of the variational mode decomposition (VMD) technique [13] to process pulse-like seismic signals. Recently, Feng et al. [16] have followed this approach and introduced some revisions. The VMD technique was proven successfully to decompose near-fault seismic ground velocity records and to identify the embedded impulsive modes together with the corresponding pulse period. This approach is here applied to process independently two components of the near-fault seismic ground motion, namely the horizontal fault-normal velocity and the vertical velocity. The interested reader is referred to previous works [16, 51] for more details about the application of the VMD technique to near-fault pulse-like seismic signals. Anyway, other suitable techniques for processing pulse-like seismic ground motion records can be employed for this task.

The consideration of the fault-normal component only of the horizontal shaking is motivated by past researches about the response of seismic isolators under near-fault earthquakes, which is the loading condition

of interest for the present study. In fact, Jangid and Kelly [25] found that the maximum seismic isolator response under near-fault earthquakes mainly occurs in the fault-normal direction while the contribution due to the parallel component can be neglected. For the sake of completeness, it is pointed out that some recent researches have also found that the maximum ductility demand does not always occur in the fault-normal direction and proposed a way to identify the horizontal orientation of the strongest velocity pulses causing the maximum response [31].

The original methodology presented by Quaranta and Mollaioli [51] is slightly revised in the present work in order to further improve the accuracy of the dominant pulse identification procedure. Key elements of the whole procedure are presented in the following. According to the VMD technique, the bandwidth of a signal mode is determined through the following procedure:

- compute the analytical signal for each mode using the Hilbert transform in such a way to obtain an unilateral frequency spectrum;
- shift the mode's frequency spectrum to baseband for each mode, by mixing with an exponential tuned to the respective estimated center frequency;
- estimate the bandwidth using the H1 Gaussian smoothness of the demodulated signal (i.e., squared L2-norm of the gradient).

This, in turn, requires the solution of the following constrained variational problem:

$$\begin{aligned} \min_{v_k,\omega_k} &\left\{ \sum_{k=1}^{N} \left\| \partial_t \left[\left(\delta(t) + \frac{\mathrm{j}}{\pi t} \right) * v_k \right] e^{-\mathrm{j}\omega_k t} \right\|_2^2 \right\}, \\ &\text{s.t.} \sum_k v_k = v \end{aligned} \tag{1}$$

where v is the signal to be decomposed (i.e., seismic ground motion velocity along the horizontal fault-normal direction or the vertical direction), v_k is the kth mode and ω_k the corresponding center pulsation ($k = 1, \ldots, N$, in which N is the number of modes), $\delta(\cdot)$ is the Dirac delta operator and $*$ is the convolution operator. Moreover, t is the time variable. The mathematical programming problem given by Eq. (1) is solved by converting the original constrained optimization into an unconstrained one. Lagrangian multipliers and a quadratic penalty term are employed to this end. So doing, the following augmented Lagrangian $\mathcal{L}$ is obtained:

$$\begin{aligned} \mathcal{L}(v_k, \omega_k, \lambda) =& \alpha \sum_{k=1}^{N} \left\| \partial_t \left[\left(\delta(t) + \frac{\mathrm{j}}{\pi t} \right) * v_k \right] e^{-\mathrm{j}\omega_k t} \right\|_2^2 \\ &+ \left\| v - \sum_{k=1}^{N} v_k \right\|_2^2 + \left\langle \lambda, v - \sum_{k=1}^{N} v_k \right\rangle, \end{aligned} \tag{2}$$

where λ is the Lagrangian multiplier and α is a parameter that rules the fidelity level. Hence, the solution of the variational problem in Eq. (1) is the saddle point of $\mathcal{L}$ given by Eq. (2), and this is obtained through

a sequence of iterative sub-optimizations named alternate direction method of multipliers. This iterative procedure can be stopped once the following convergence criterion is fulfilled:

$$\sum_{k=1}^{N} \left\| {}^{i+1}v_k - {}^{i}v_k \right\|_2^2 / \left\| {}^{i}v_k \right\|_2^2 < \epsilon, \tag{3}$$

where i is the iteration counter and ϵ is the selected tolerance. Although the essentials of the VMD technique have been shortly summarized in the time domain, it is pointed out that the complete algorithm is more efficiently implemented in the spectral domain. Once the original seismic ground motion velocity is decomposed, the resulting modes can be analyzed by employing a suitable index that quantifies their impulsiveness to identify the dominant pulse-like waveform, if any, and the corresponding pulse period.

In order to enhance the accuracy of the dominant pulse-like waveform identification, the original methodology proposed by Quaranta and Mollaioli [51] is slightly revised accounting for previous works by Menun and Fu [43] and Chang et al. [5], who have identified the dominant impulsive mode by minimizing directly the difference between a numerical pulse model and the original velocity time-history of the seismic ground motion. A similar idea is here implemented, but considering the signal modes extracted by means of the VMD technique instead of the original record. Considering the single signal modes instead of the whole original record strongly reduces the influences due to the contribution of signal frequencies corresponding to other pulse- and/or nonpulse-like modes when looking for the dominant impulsive one.

Accordingly, once the original seismic ground motion velocity has been decomposed, each extracted mode v_k is fitted with a numerical pulse-like waveform. In the present study, the numerical model proposed by Mavroeidis and Papageorgiou [37] is considered:

$$\hat{v}_p(\theta) = \begin{cases} A_p \dfrac{1}{2}\left[1 + \cos\left(\dfrac{2\pi}{T_p\gamma}(t - t_0)\right)\right] \cos\left(\dfrac{2\pi(t - t_0)}{T_p} + \nu\right) & \text{if } t_0 - \dfrac{T_p\gamma}{2} \leq t \leq t_0 + \dfrac{T_p\gamma}{2} \\ 0 & \text{otherwise} \end{cases}, \tag{4}$$

where $\theta = \{A_p, T_p, t_0, \nu, \gamma\}$ is the model parameters vector. Here, A_p controls the amplitude, T_p is pulse period of the numerical waveform, t_0 specifies the epoch of the envelope's peak, ν is the phase ($\nu = 0$ and $\nu = \pm\pi/2$ correspond to symmetric and antisymmetric signals, respectively), $\gamma > 1$ is a parameter that defines the oscillatory behavior of the signal (the larger is γ, the larger is the number of zero-crossing). The model parameters vector θ for each mode, namely θ_k, is obtained by fitting the corresponding waveform with the numerical waveform given by Eq. (4). This requires the solution of the following optimization problem $\forall k$:

$$\min_{\theta_\ell \leq \theta_k \leq \theta_u} \{MSE_k(\theta_k)\}, \tag{5}$$

in which $MSE_k(\theta_k) = MSE(\hat{v}_p(\theta_k), v_k)$, where $MSE(\cdot, \cdot)$ is the mean squared error operator. Moreover, θ_ℓ and θ_u are the lower and upper bound of the search space for θ_k, respectively. As it has been already pointed out by Menun and Fu [43], this search space can exhibit multiple local optima, thereby making

local optimizers ineffective. Following Menun and Fu [43], therefore, this problem is resolved by using soft computing based optimizers with global search capability [54]. Let $\hat{v}_p(\theta_k)$ be the candidate dominant impulsive mode obtained $\forall k$ from the solution of Eq. (5). In order to determine whether it is an impulsive mode, a suitable index must be used. The pulse indicator proposed by Baker [3] is here adopted as follows:

$$PI_k(\theta_k) = \frac{1}{1+\exp\left(-23.3+14.6\rho_{PGV}(\theta_k)+20.5\rho_{E_v}(\theta_k)\right)}, \tag{6}$$

where $\rho_{PGV}(\theta_k)$ is the peak ground velocity of the residual record divided by the original record's peak ground velocity whereas $\rho_{E_v}(\theta_k)$ is the energy of the residual record divided by the original record's energy (herein, the energy is computed as the cumulative squared velocity). The residual record is obtained by removing the kth candidate dominant impulsive mode $\hat{v}_p(\theta_k)$ from the original record v. The dominant impulsive mode v_p is thus identified as $p = \text{argmax}_k\{PI_k(\theta_k)\}$ subjected to $PI_k(\theta_k) \geq PI_{\min}$, where $PI_{\min}$ is a suitable threshold values of pulse indicator. The pulse period of the dominant impulsive mode is then defined as $T_p = 2\pi/\omega_p$, where ω_p is the center pulsation of the dominant impulsive mode v_p. According to Baker [3], $0.15 \leq PI_{\min} \leq 0.85$ where $PI_{\min} = 0.15$ and $PI_{\min} = 0.85$ can be interpreted as "soft threshold" and "hard threshold" for the impulsiveness level, respectively. It is pointed out that other suitable pulse indicators can be employed for this task.

3. Numerical modeling of high-damping rubber bearings

High-damping-rubber bearings (HDRBs) are largely employed for seismic isolation. Many models with different complexity levels have been proposed to simulate their behavior, spanning from equivalent linear models [17, 33] to hysterestic models [46, 52]. A key aspect that influences their performance under earthquake is the interaction of the horizontal response with the axial load, which thus deserves proper consideration. The present study is meant at investigating the displacement demand of circular HDRBs in buildings isolation through a quite large statistical analysis. This calls for a numerical model able to take into account both horizontal and vertical isolator response by means of effective, yet simple, rules involving few well-established parameters having a clear physical meaning. The two-spring-two-dashpot model for HDRBs proposed by Mazza and Vulcano [42] is deemed especially suitable for this goal, and thus it is implemented in the present study. The main features of this model are summarized in the following, whereas more details and further pertinent references can be found in the original work by Mazza and Vulcano [42].

The nonlinear HDRB model consists of a spring-dashpot unit for simulating the horizontal behavior of the device and another spring-dashpot module for taking into account the effects of the axial load. Spring and dashpot within this numerical model work in parallel along both directions.

Let K_H and u_H be the actual stiffness and the relative displacement of the spring in the horizontal direction, respectively, its nonlinear force-displacement relationship F_K–u_H is defined as follows:

$$F_K = K_H u_H = K_H^0 \left[1-(P/P_{cr})^2\right] u_H, \tag{7}$$

in which K_H^0 is the nominal horizontal stiffness of the HDRB, P is the total axial load and P_{cr} the corresponding critical value. The value of K_H^0 is given by:

$$K_H^0 = GA/t_r, \tag{8}$$

where G is the shear modulus, A the cross-section area of the single elastomeric layer, and t_r the total thickness of the rubber. Based on the linear stability analysis of multilayer elastomeric bearings, P_{cr} is determined as follows:

$$P_{cr} = \pi G S_1 S_2 \sqrt{A A_r}/(2\sqrt{2}), \tag{9}$$

where S_1 and S_2 the shape factors of the HDRB. Moreover, A_r is the reduced effective cross-section area (i.e., the area of overlap between the top and bottom of the isolator), which is defined as follows:

$$A_r = (\delta - \sin\delta)\,\phi_b^2/4, \tag{10a}$$

$$\delta = 2\arccos\left(|u_H|/\phi_b\right). \tag{10b}$$

The shape factors are defined as $S_1 = \phi_b/(4t)$ and $S_2 = \phi_b/t_r$, where ϕ_b and t are the bearing diameter and the thickness of the single layer of rubber, respectively.

The horizontal behavior simulation is complemented with a linear viscous dashpot. Therefore, let C_H and $\dot{u}_H$ be the actual equivalent viscous damping and the relative velocity of the dashpot in the horizontal direction, respectively, its linear force-velocity relationship F_C–$\dot{u}_H$ is defined as follows:

$$F_C = C_H \dot{u}_H = \xi_H K_H^0 T_{1H} \dot{u}_H/\pi, \tag{11}$$

where ξ_H and T_{1H} are the equivalent viscous damping ratio and the fundamental vibration period in the horizontal direction, respectively.

On the other hand, let K_V and u_V be the actual stiffness and the relative displacement of the spring in the vertical direction, respectively, its nonlinear force-displacement relationship P_K–u_V is defined accounting for the second-order geometric effect as follows:

$$P_K = \frac{K_V^0\left(u_V - \dfrac{\alpha_b}{\alpha_K^0}\dfrac{16}{\pi^2\phi_b S_2}u_H^2\right)}{1 + 48\left(\dfrac{u_H}{\pi\phi_b}\right)^2}, \tag{12}$$

where $\alpha_b = h_b/t_r$, with h_b the total height of the bearing. Moreover, $\alpha_K^0 = K_V^0/K_H^0$, in which K_V^0 is the nominal vertical stiffness given by:

$$K_V^0 = E_c A/t_r, \tag{13}$$

where E_c is the compression modulus of the rubber-steel composite bearing.

Finally, the vertical behavior simulation is complemented with a linear viscous dashpot following a similar approximation adopted previously for the horizontal direction. Therefore, let C_V and $\dot{u}_V$ be the actual

equivalent viscous damping and the relative velocity of the dashpot in the vertical direction, respectively, its linear force-velocity relationship P_C–$\dot{u}_V$ is defined as follows:

$$P_C = C_V \dot{u}_V = \xi_V K_V^0 T_{1V} \dot{u}_V / \pi, \tag{14}$$

where ξ_V and T_{1V} are the equivalent viscous damping ratio and the fundamental vibration period in the vertical direction, respectively. It can be inferred from Eq. (7) and Eq. (12) that horizontal and vertical stiffness isolator are directly coupled each other, whereas the coupling in terms of damping is not explicit in Eq. (11) and Eq. (14). Although this model was later subjected to slight revisions [41], the original model by Mazza and Vulcano [42] is a good trade-off in terms of complexity and accuracy for the goals of the following statistical analysis.

The displacement demand of HDRBs is herein analyzed in the context of buildings isolation. Specifically, it is considered a symmetric superstructure subjected to uniform base excitation (with no overtuning or tilting) represented by a horizontal fault-normal pulse-like seismic ground motion component and a vertical shaking. Following Kulkarni and Jangid [30], the superstructure is idealized as a rigid body. Therefore, the base-isolated structure is modeled ultimately as a two-degrees-of-freedom system. The idealization of base-isolated superstructures as rigid bodies is routinely used for the analysis of isolation systems [9, 25] and relies on the evidence that base isolation displacements are usually much higher than those of the superstructure. Kulkarni and Jangid [30] demonstrated that such assumption can accurately predict the bearing displacements, thereby resulting in line with the goals of the following statistical analysis and making it possible the generalization of its conclusions. On the other hand, it is highlighted that the hypothesis of rigid body response for base-isolated structures may not be fully justified for predicting the superstructure response [30]. This limitation, however, is not relevant for the present work, which is meant at investigating the maximum displacement of elastomeric bearings only. Figure 1 illustrates the numerical modeling approach herein adopted in order to evaluate the effect of the vertical shaking (i.e., pulse- or nonpulse-like) on the maximum horizontal displacement of elastomeric bearings.

4. Numerical investigation

4.1. Pulse extraction and pulse period estimation

The database of seismic records for the present work is based on time histories retrieved from Engineering Strong-Motion (ESM) database, Italian Accelerometric Archive (ITACA), Pacific Earthquake Engineering Research Center (PEER) Ground Motion Database, Consortium of Organizations for Strong Motion Observation Systems (COSMOS), Center for Engineering Strong Motion Data (CESMD). Post-processed seismic records have been downloaded from these repositories. The complete list of analyzed seismic records is provided in Appendix. While all the fault-normal horizontal components of these seismic events embed an

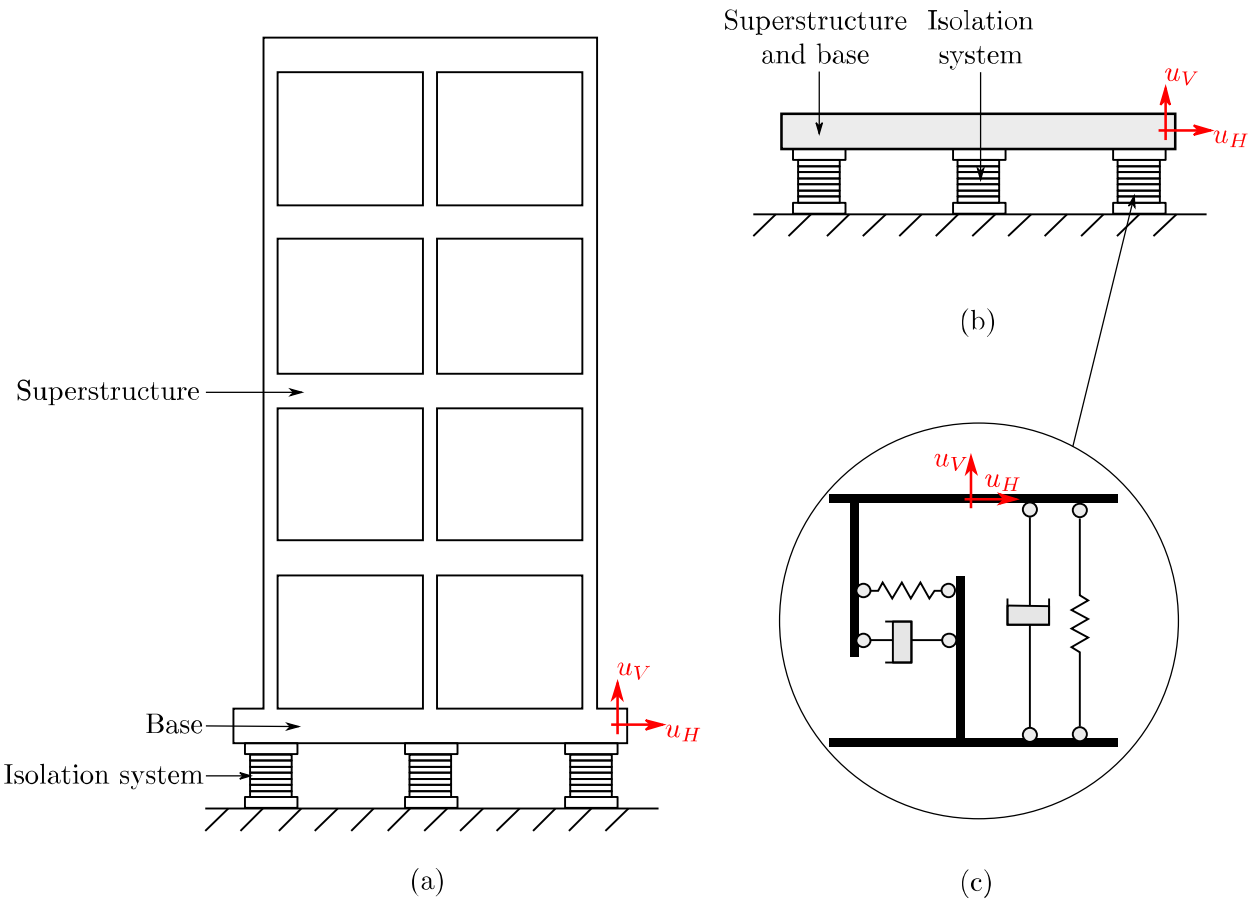

Figure 1: Numerical modeling for the assessment of the maximum horizontal displacement of elastomeric bearings: flexible superstructure with elastomeric bearings at the base (a); adopted rigid body idealization (b) after Kulkarni and Jangid [30]; two-spring-two-dashpot nonlinear model of the HDRB (c) after Mazza and Vulcano [42].

impulsive mode, the vertical component may be or not pulse-like. This list provides details about which vertical seismic components have been classified as pulse-like according to the implemented procedure as well as on the forward directivity effect. Almost all seismic signals have been recorded at a Joyner-Boore distance less than 25 km and on soils whose shear wave velocity in the upper 30 m layer is less 500 m/s. A very few of them exhibit a permanent displacement offset and are affected by fling step effect.

Figure 2 shows the peak ground acceleration values along the horizontal fault-normal direction PGA_H and that along the vertical direction PGA_V, together with the ratio between them $\mathrm{PGA}_H/\mathrm{PGA}_V$. Similarly, Fig. 2 also illustrates the peak ground velocity values along the horizontal fault-normal direction PGV_H and that along the vertical direction PGV_V, together with the ratio between them $\mathrm{PGV}_H/\mathrm{PGV}_V$. All these kinematic quantities are plotted as function of the earthquake moment magnitude M. While all the events under consideration have a pulse-like fault-normal seismic ground motion component, they are disaggregated into seismic events with or without an impulsive vertical shaking. It can be inferred from Fig.

2 that $\mathrm{PGA}_H > \mathrm{PGA}_V$ in several seismic events under consideration, but there is a non negligible number of earthquakes for which the opposite condition takes place. On the other hand, the condition $\mathrm{PGV}_H > \mathrm{PGV}_V$ holds for almost all the seismic events under consideration, and the highest values of the ratio $\mathrm{PGV}_H/\mathrm{PGV}_V$ usually corresponds to earthquakes characterized by a nonpulse-like vertical component of the ground motion. For the collected set of seismic events, it is also deduced that $\mathrm{PGV}_H/\mathrm{PGV}_V > \mathrm{PGA}_H/\mathrm{PGA}_V$ on average.

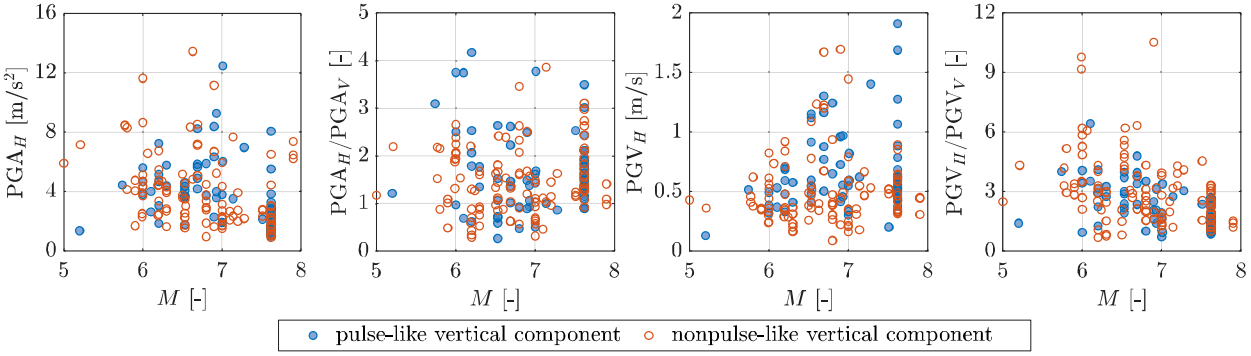

Figure 2: Distribution of peak ground acceleration and velocity values in the fault-normal and vertical component as function of the earthquake magnitude.

Figure 3 provides some information about the focal mechanisms within the considered database of seismic records. It can be deduced from Fig. 3 that several seismic events with a pulse-like seismic ground motion along the fault-normal and the vertical direction are originated from a strike-slip mechanism and, to a less extent, from a reverse mechanism. The apparent large number of such kind of seismic events generated by a reverse–oblique mechanism in Fig. 3 is a distortion due to a cluster that refers to a single earthquake, namely the 1999 Chi-Chi earthquake. In this sense, the present analysis agrees with the preliminary conclusions drawn by Ertuncay and Costa [15], who have already pointed out the existence of vertical impulsive signals in the seismic ground motions recorded during the 1999 Chi-Chi earthquake.

Figures 4-9 provide a short overview about the outputs of the implemented approach for pulse extraction. Figure 4 refers to the 1979 Imperial Valley earthquake. The peak ground acceleration of the horizontal fault normal component PGA_H is slightly lower than the corresponding value measured along the vertical component PGA_V. On the other hand, the peak ground velocity of the horizontal fault normal component PGV_H is much larger than the corresponding value measured along the vertical component PGV_V. The fault-normal component of the seismic ground motion is pulse-like (with a pulse index equal to 1), and the corresponding pulse period value is $T_{p,H} = 4.37$ s. This value is in very good agreement with the alternative estimates obtained by Quaranta and Mollaioli [51] according to Baker [3] (i.e., $T_{p,H} = 4.80$ s), [5] (i.e., $T_{p,H} = 4.20$ s), and Mimoglou et al. [44] (i.e., $T_{p,H} = 4.24$ s). Conversely, the vertical component of the seismic ground motion is nonpulse-like (the maximum pulse index was found equal to 0.05).

The seismic records due to the 1979 Coyote Lake earthquake are analyzed in Figure 5. In such case, it

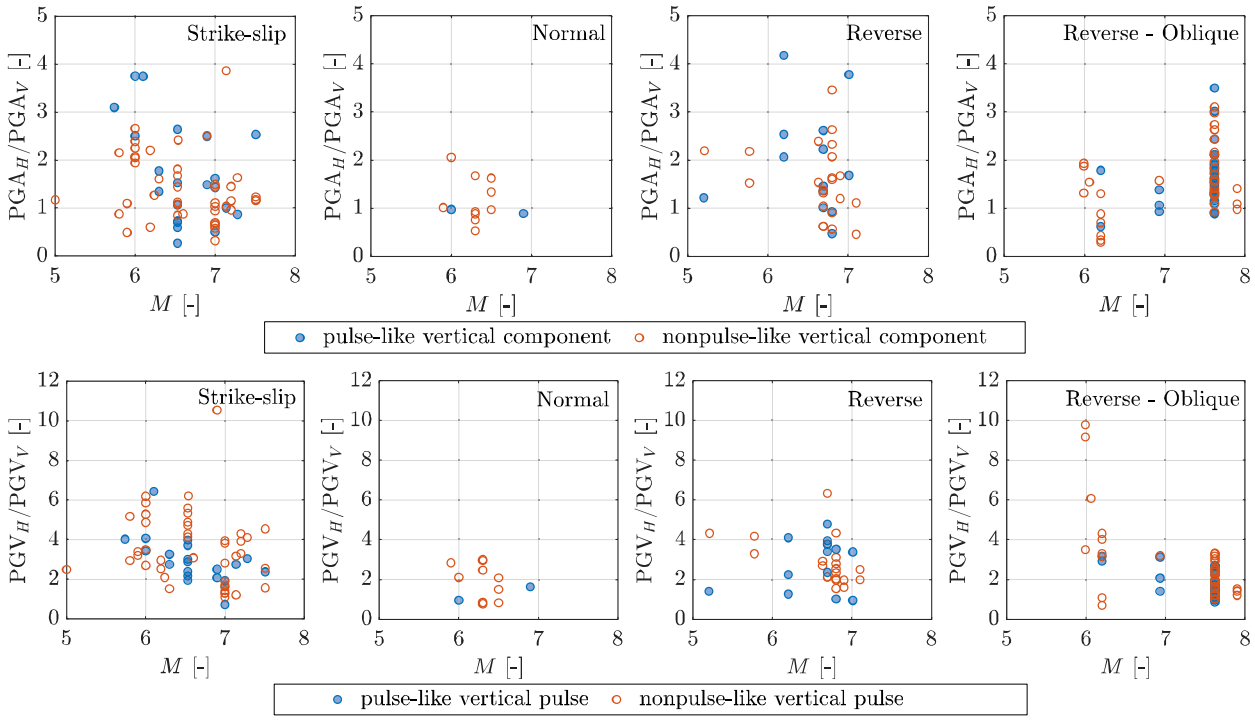

Figure 3: Distribution of the ratio between peak ground acceleration (top) and velocity (bottom) values in the fault-normal and vertical component as function of the earthquake magnitude for different focal mechanisms.

is found that the fault-normal component as well as the vertical component of the seismic ground motion are both pulse-like (with a pulse index almost equal to 1 for both records). The calculated value of the pulse period along the fault-normal direction is $T_{p,H} = 1.07$ s, which results in good agreement with the alternative estimates obtained by Quaranta and Mollaioli [51] according to Baker [3] (i.e., $T_{p,H} = 1.21$ s), Chang et al. [5] (i.e., $T_{p,H} = 1.00$ s), and Mimoglou et al. [44] (i.e., $T_{p,H} = 0.92$ s). This is rather lower than the pulse period along the vertical direction, whose value has been found equal to $T_{p,V} = 1.44$ s.

Figure 6 provides the results corresponding to the analysis of the 2004 Parkfield earthquake. The fault-normal component is characterized by an impulsive waveform (with a pulse index almost equal to 1), and the corresponding pulse period is $T_{p,H} = 1.07$ s. The good agreement with the results obtained by Quaranta and Mollaioli [51] using the approaches proposed by Baker [3] (i.e., $T_{p,H} = 1.15$ s), Chang et al. [5] (i.e., $T_{p,H} = 1.10$ s), and Mimoglou et al. [44] (i.e., $T_{p,H} = 0.92$ s) is confirmed once again. The vertical component is also pulse-like (with a pulse index equal to 0.94). In such case, the pulse period along the fault-normal direction is rather larger than the pulse period along the vertical direction, whose value has been found equal to $T_{p,V} = 0.77$ s.

The 2008 Ölfus earthquake is analyzed in Figure 7. Both fault-normal and vertical components of the seismic ground motion have been found to be pulse-like (with a pulse index almost equal to 1), and

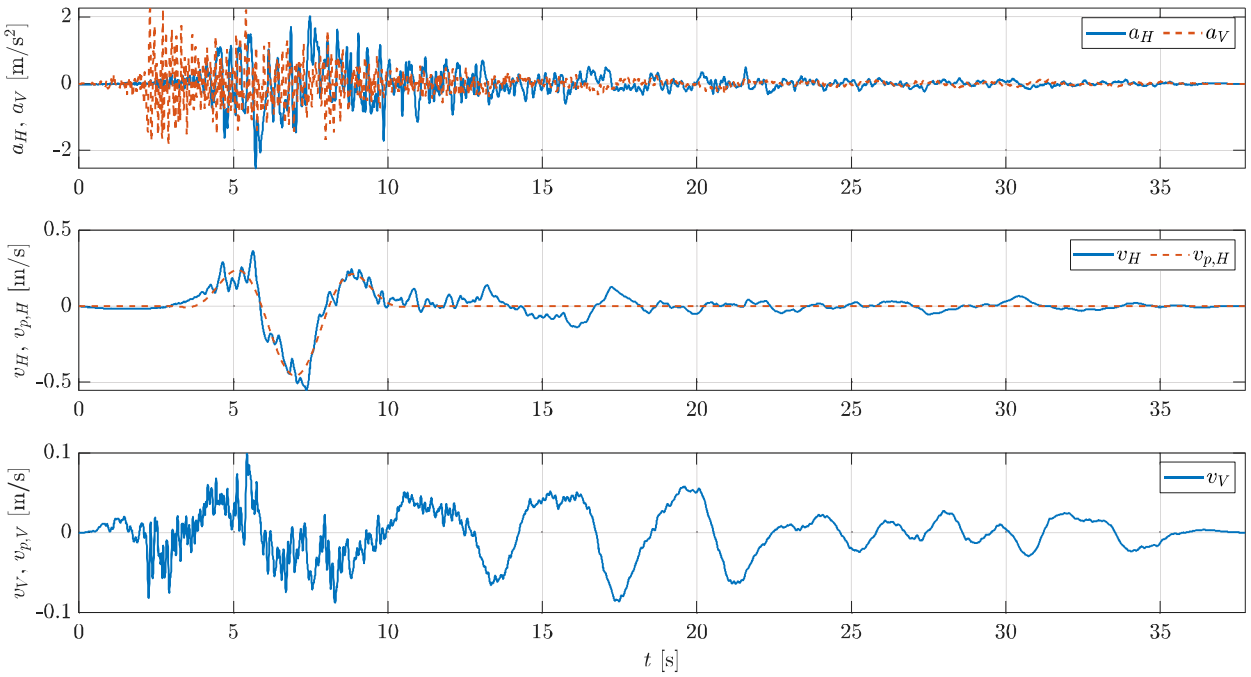

Figure 4: 1979 Imperial Valley earthquake (Holtville Post Office station): accelerograms and dominant pulse extraction in the fault-normal and vertical direction.

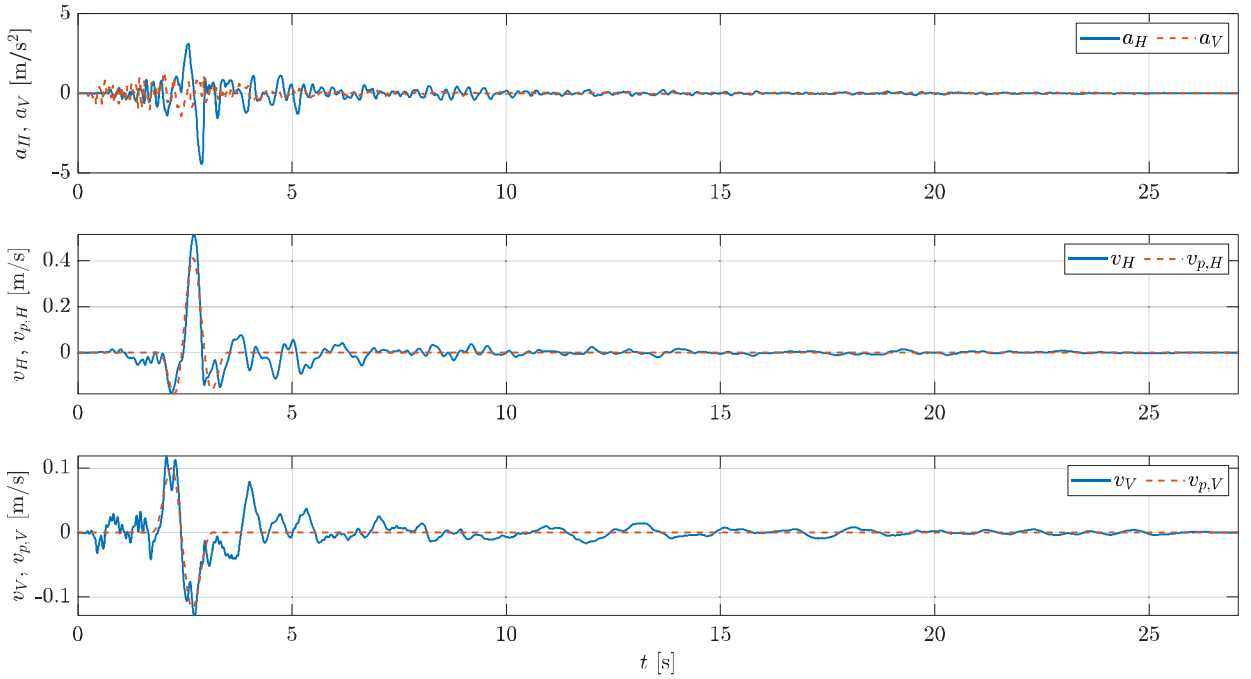

Figure 5: 1979 Coyote Lake earthquake (Gilroy Array #6 station): accelerograms and dominant pulse extraction in the fault-normal and vertical direction.

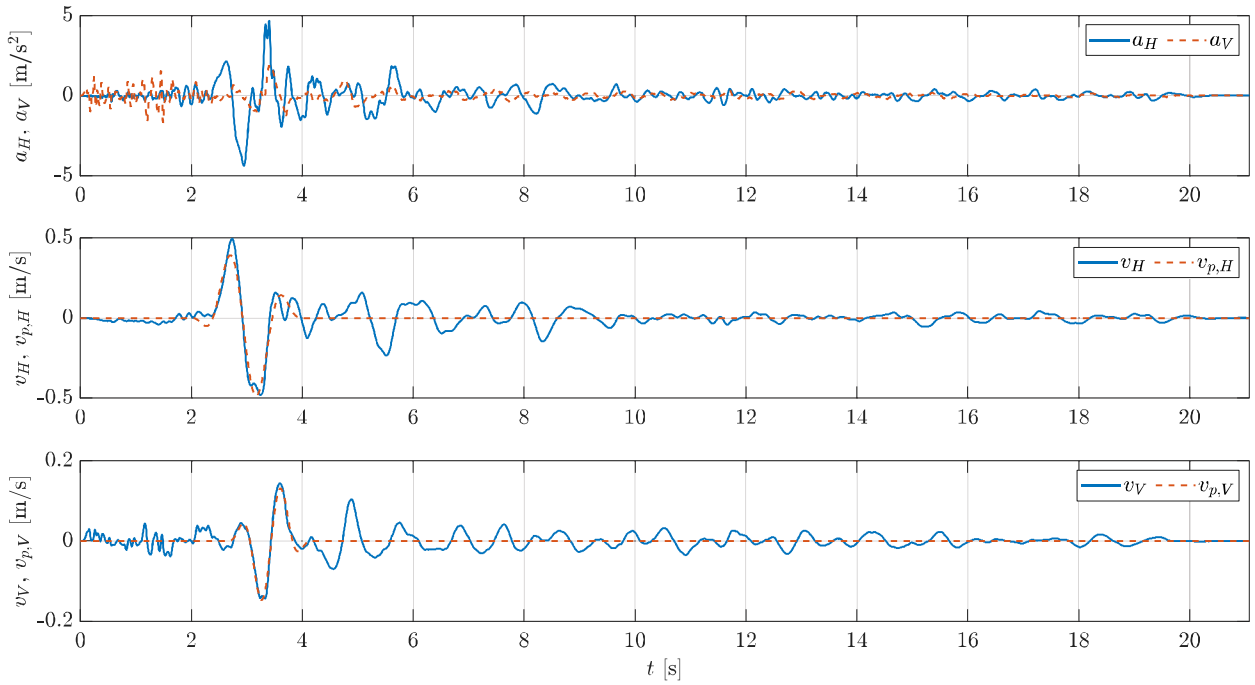

Figure 6: 2004 Parkfield earthquake (Cholame 2W station): accelerograms and dominant pulse extraction in the fault-normal and vertical direction.

the estimated values of the corresponding pulse period are $T_{p,H} = 1.21$ s and $T_{p,V} = 2.29$ s, respectively. Therefore, the pulse period in the vertical direction is about two times the one in the fault-normal direction. It is noted that Quaranta and Mollaioli [51] found a larger scattering about the pulse period value along the horizontal fault-normal direction when the estimation is performed according to Baker [3] (i.e., $T_{p,H} = 1.40$ s), Chang et al. [5] (i.e., $T_{p,H} = 0.90$ s), or Mimoglou et al. [44] (i.e., $T_{p,H} = 3.23$ s).

While all previous seismic events with a pulse-like vertical component in Figs. 5-7 are originated from a strike-slip focal mechanism and are characterized by low pulse period values, those in Figs. 8-9 are produced from a non-strike-slip focal mechanism and present mid-high pulse period values. Both Fig. 8 and Fig. 9 refer to the 1999 Chi-Chi earthquake, which has occurred through a reverse-oblique focal mechanism. The analysis of the seismic records shows that the fault-normal component as well as the vertical component of the seismic ground shaking have an impulsive waveform (with pulse index values almost equal to 1 for both records). Specifically, the fault-normal component and the vertical component illustrated in Fig. 8 have pulse period values equal to $T_{p,H} = 5.20$ s and $T_{p,V} = 3.57$ s, respectively. The pulse period value in the fault-normal component is in-between the results obtained by Quaranta and Mollaioli [51] following the methods proposed by Baker [3] (i.e., $T_{p,H} = 5.15$ s), Chang et al. [5] (i.e., $T_{p,H} = 4.00$ s), and Mimoglou et al. [44] (i.e., $T_{p,H} = 5.44$ s). On the other hand, the pulse-like components of the seismic ground records in Fig. 9 have a pulse period equal to $T_{p,H} = 8.62$ s and $T_{p,V} = 4.84$ s, respectively. Once again, a large scattering exists among the estimates of the pulse period in the fault-normal direction as obtained by Quaranta and

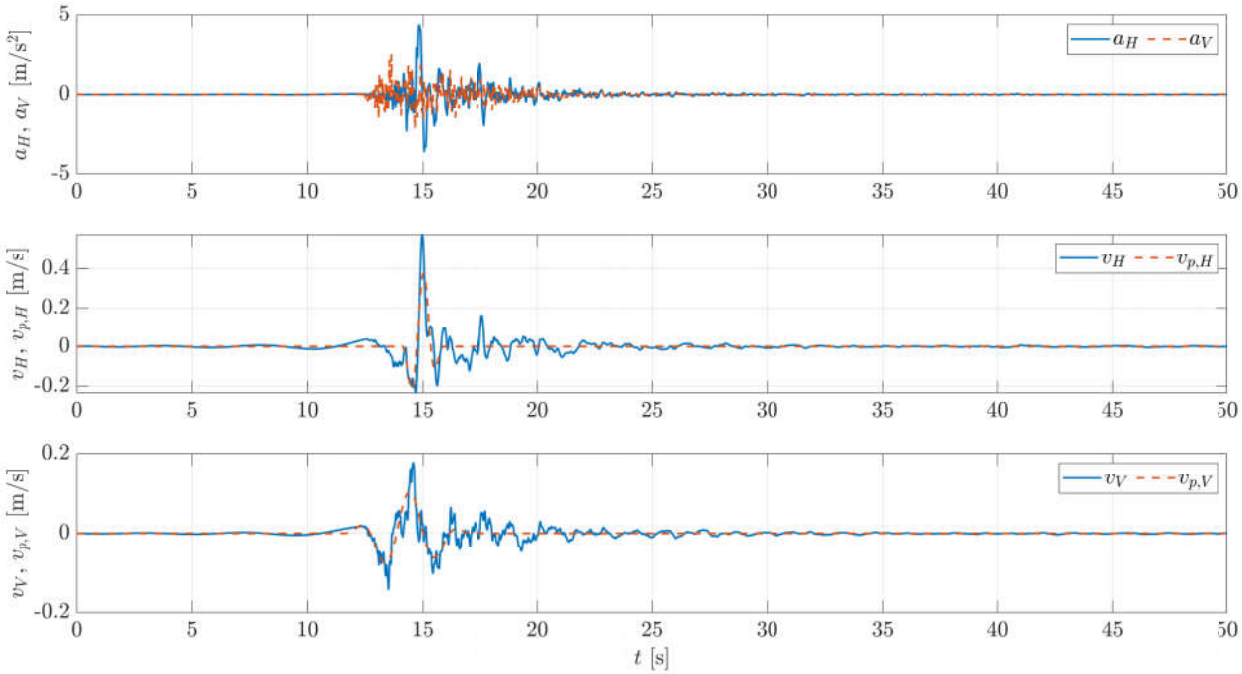

Figure 7: 2008 Ölfus earthquake (Selfoss City Hall station): accelerograms and dominant pulse extraction in the fault-normal and vertical direction.

Mollaioli [51] following the methods proposed by Baker [3] (i.e., $T_{p,H} = 10.04$ s), Chang et al. [5] (i.e., $T_{p,H} = 5.60$ s), and Mimoglou et al. [44] (i.e., $T_{p,H} = 9.47$ s). Overall, it is possible to infer from Figs. 8-9 that the pulse period along the fault-normal direction is significantly larger than the corresponding value estimated in the vertical direction.

For seismic events having a pulse-like waveform along the fault-normal direction and the vertical one, Fig. 10 analyzes the ratio between the corresponding pulse periods $T_{p,H}/T_{p,V}$. Figure 10 highlights that such seismic events are usually characterized by the condition $0.5 \leq T_{p,H}/T_{p,V} \leq 2$. Moreover, the condition $T_{p,H}/T_{p,V} > 1$ seems the most recurrent one, which implies that the vertical pulse is usually characterized by a higher frequency than the impulsive waveform along the horizontal direction. This is in agreement with the general mechanism underlying the propagation of seismic waves. In fact, the wavelength of compressive P-waves (to which the vertical component of the ground motion is mainly associated) is generally shorter than that of shear S-waves (which are the main cause of the horizontal shaking), and thus the seismic ground motion usually exhibits a higher frequency content in the vertical direction rather than along the horizontal one [14].

It is also shown in Fig. 10 that $T_{p,H}/T_{p,V}$ is quite well linearly correlated to $T_{p,H}$. Conversely, it is also deduced from Fig. 10 that $T_{p,H}/T_{p,V}$ is basically uncorrelated to $T_{p,V}$. Based on a standard regression, the

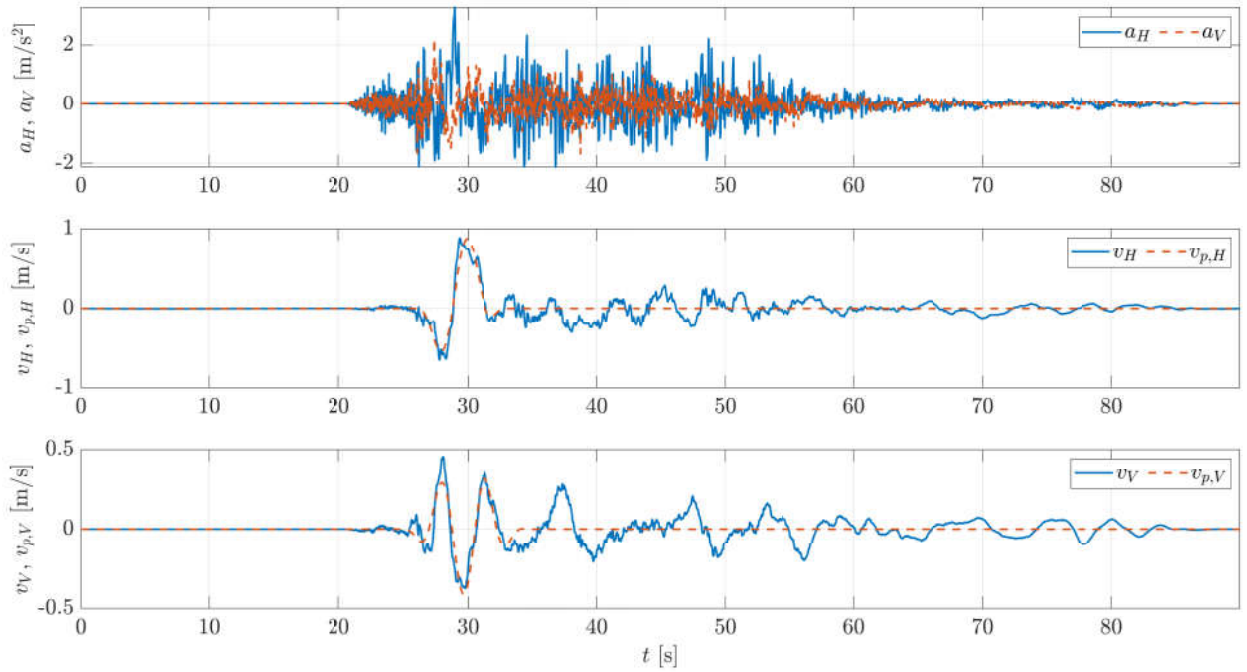

Figure 8: 1999 Chi-Chi earthquake (TCU075 station): accelerograms and dominant pulse extraction in the fault-normal and vertical direction.

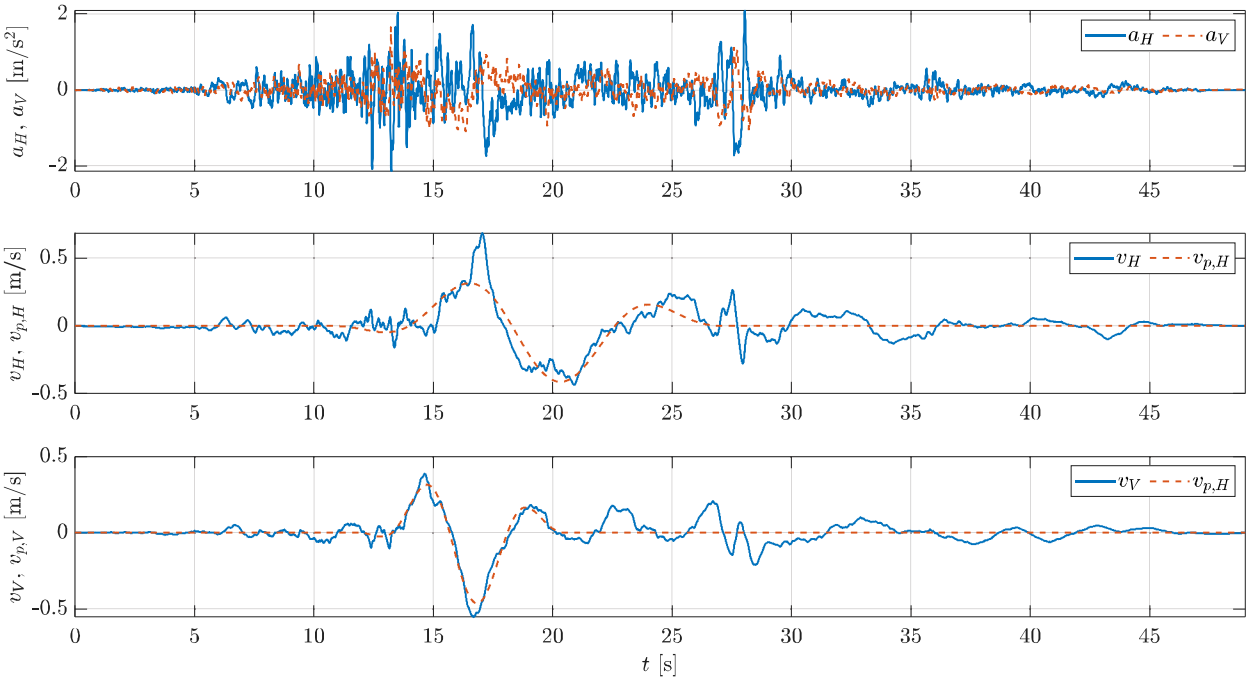

Figure 9: 1999 Chi-Chi earthquake (TCU101 station): accelerograms and dominant pulse extraction in the fault-normal and vertical direction.

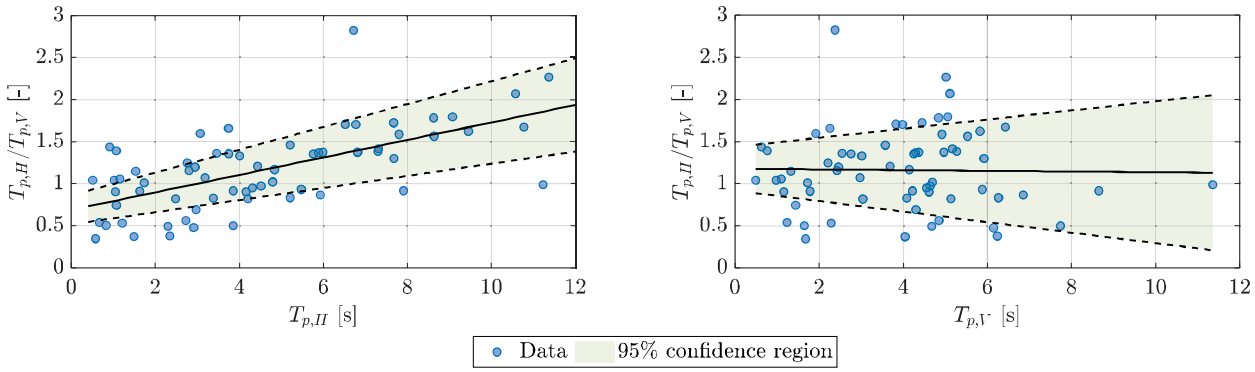

Figure 10: Correlation of the ratio between the pulse periods in the fault-normal and vertical component as function of the pulse period value in a single direction.

following relationship is proposed:

$$\frac{T_{p,H}}{T_{p,V}} = b_0 + b_1 T_{p,H}, \tag{15}$$

where b_0 [-] and b_1 [1/s] are the regression coefficients listed in Tab. 1.

Table 1: Regression coefficients for Eq. (15).

Regression coefficient	Value	95% confidence interval
b_0 [-]	0.6877	$[0.5155, 0.8599]$
b_1 [1/s]	0.1040	$[0.0721, 0.1359]$

Once the pulse period in the fault-normal direction $T_{p,H}$ for a given site is thus estimated using one of the available predictive formulations that correlates its value to relevant seismological data [3, 6, 24, 37, 51], Eq. (15) allows to calculate the pulse period in the vertical direction as well (it is pointed out that the probability of occurrence of an impulsive vertical component of the seismic ground motion at the site is not investigated).

4.2. Effect of vertical pulse on the seismic isolator response

It is now investigated whether the waveform of the vertical shaking (i.e., pulse or nonpulse-like) has some effects on the displacement response of HDRB under a fault-normal pulse-like seismic ground motion. In the attempt to shed a light on this issue, the maximum absolute horizontal displacement u_H^{VP} of the HDRB is first calculated under earthquake records characterized by a fault-normal impulsive ground motion and a pulse-like vertical shaking. The final result is thus compared to u_H^{nVP}, that is the maximum absolute horizontal displacement of the HDRB calculated under earthquake records characterized by a horizontal impulsive ground motion and a nonpulse-like vertical shaking. The key parameter for the evaluation of the effect of the vertical pulse on the seismic isolator response is thus the ratio between the corresponding maximum absolute displacements, i.e. $\Delta = u_H^{\mathrm{VP}}/u_H^{\mathrm{nVP}}$. It is recalled that the maximum absolute horizontal

displacement of the HDRB is estimated under the assumption that the superstructure is idealized as a rigid body, and then the base-isolated structure is modeled ultimately as a two-degree-of-freedom system, in agreement with the conclusions drawn by Kulkarni and Jangid [30].

In order to perform this comparative assessment of the device response, selection and scaling criteria must be defined. In fact, it must be specified how seismic events with pulse-like shaking in the horizontal direction only are selected and then scaled for each (reference) earthquake characterized by an impulsive waveform along both fault-normal and vertical direction. In this regard, several studies have pointed out that the response under horizontal pulse-like seismic ground motion of structural systems and protection devices is in some way influenced by the pulse period $T_{p,H}$. Therefore, for each earthquake characterized by an impulsive waveform along the fault-normal direction and the vertical direction, seismic events with nonpulse-like vertical shaking are selected in such a way that the relative difference between the corresponding values of $T_{p,H}$ is no larger than 10%. If a non-empty pool of seismic events with nonpulse-like vertical shaking is thus available after the selection procedure, then each record must be scaled in order to make the comparative assessment as less biased as possible in terms of intensity. Unfortunately, accelerograms scaling in case of near-fault pulse-like seismic ground motion is an open issue yet [39]. Scaling based on peak ground acceleration seems the most widespread in the current literature for the analysis of general structural systems under near-fault pulse-like earthquake records [19, 45]. This holds especially true for the applications relevant for the present study, i.e. vertical shaking and/or seismic isolation [27, 29]. Therefore, because of the lack of specialized investigations and in agreement with existing studies, PGA scaling is also adopted in the present study. It means that each selected seismic event with nonpulse-like vertical shaking is scaled in such a way that its values of PGA_H and PGA_V are equal to the corresponding ones of the (reference) earthquake characterized by an impulsive waveform along the fault-normal direction and the vertical direction. The scaling factor is constrained within the range $0.5 - 2$. This implies that the selected seismic event with nonpulse-like vertical shaking is removed from the pool prepared for the comparative analysis if one of its scaling factors (i.e., either in the horizontal or vertical direction) is less than 0.5 or larger than 2.

The definition of the device properties for the following statistical analysis is based on the study by Mazza and Vulcano [42]. Specifically, it is considered a HDRB with circular cross-section and diameter $\phi_b = 0.6$ m. Several fundamental vibration period values are considered in the horizontal direction, namely $T_{1H} = \{2.50, 2.75, 3.00, 3.25, 3.50, 3.75, 4.00\}$ s. A constant fundamental vibration period value is assumed in the vertical direction, namely $T_{1V} = 0.10$ s. The equivalent viscous damping ratios are $\xi_{1H} = 10\%$ and $\xi_{1V} = 5\%$. The shape factors are $S_1 = 18$ and $S_2 = 3$. Shear and volumetric compression moduli are $G = 0.35$ MPa and $E_b = 2000$ MPa, respectively. Motion equation is integrated via explicit Runge-Kutta formulation under the assumption of null initial conditions. Figure 11-13 illustrates some samples of the bearing response for $T_{1H} = 2.50$ s as follows: (i) the first row illustrates the seismic accelerograms

in the horizontal fault-normal direction and in the vertical direction; (ii) the second row shows the bearing horizontal displacement; (iii) the third row provides the time histories of total axial load and critical axial load. The response under the (reference) earthquake characterized by an impulsive waveform along both the fault-normal direction and the vertical direction is shown in the first column. Particularly, Fig. 11 and Figs. 12-13 provide the device response under the 1979 Coyote Lake earthquake (Gilroy Array #6 station) in Fig. 5 and the 1999 Chi-Chi earthquake (TCU075 and TCU101 station) in Figs. 8-9, respectively. On the other hand, the response under the selected and scaled seismic events with nonpulse-like vertical shaking is presented within the remaining columns. It is highlighted that the condition $u_{1H} \approx \phi_b$ in Fig. 12 leads to a premature stop of the analysis.

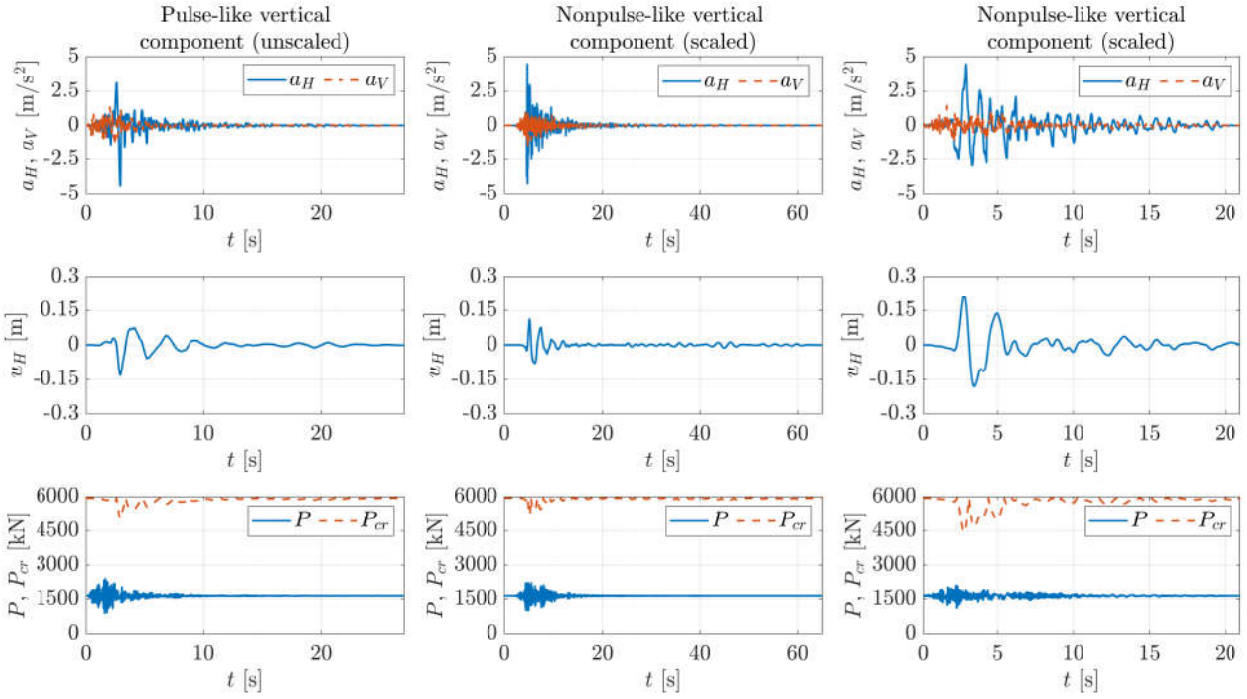

Figure 11: Analysis of the seismic bearing response subjected to pulse-like horizontal ground motion together with pulse-like (first column) and nonpulse-like (remaining columns) vertical ground motion. The seismic event with pulse-like seismic ground motion along the two directions is the 1979 Coyote Lake earthquake (Gilroy Array #6 station) analyzed in Fig. 5.

For each earthquake characterized by an impulsive waveform along the fault-normal direction and the vertical direction, Fig. 14 provides the ratio between the corresponding maximum absolute displacement of the elastomeric bearing u_H^{VP} and the one calculated for the selected and scaled earthquake records characterized by a horizontal impulsive ground motion only u_H^{nVP} (i.e., the performance index Δ) given the fundamental vibration period T_{1H}. Herein, the average value of Δ is provided considering and excluding the outlier values (an outlier corresponds to a value that is more than three scaled median absolute deviations away from the median).

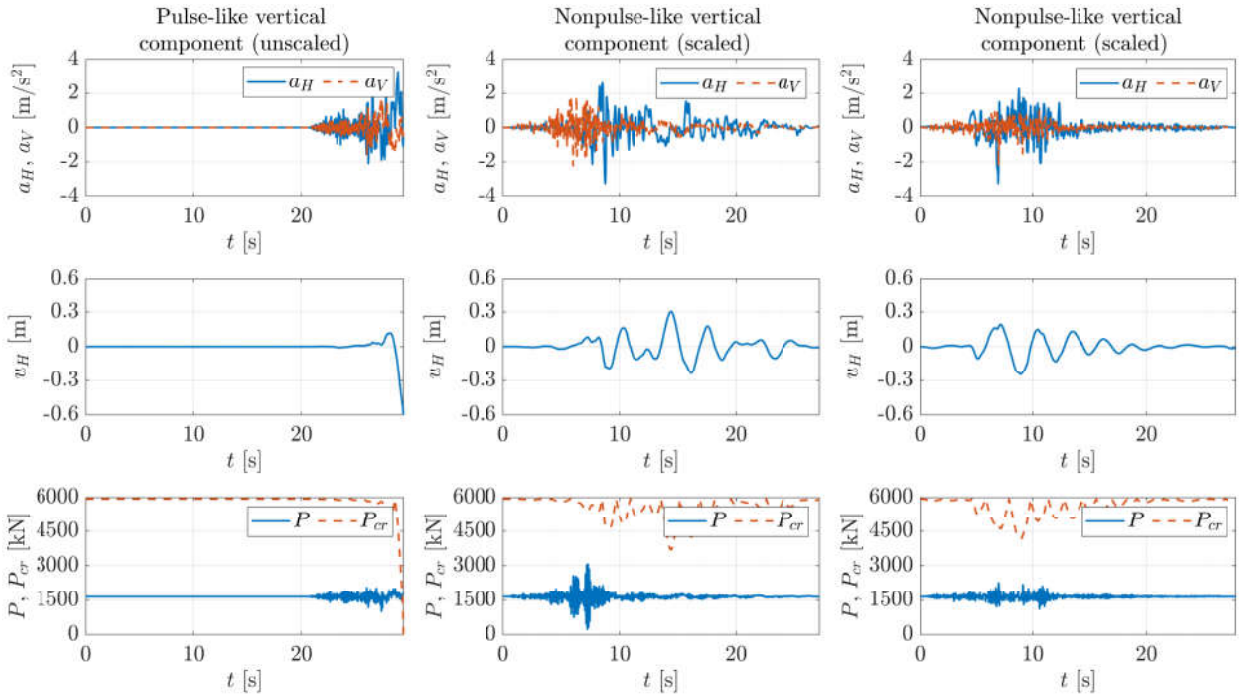

Figure 12: Analysis of the seismic bearing response subjected to pulse-like horizontal ground motion together with pulse-like (first column) and nonpulse-like (remaining columns) vertical ground motion. The seismic event with pulse-like seismic ground motion along the two directions is the 1999 Chi-Chi earthquake (TCU075 station) analyzed in Fig. 8.

Figure 14 basically reveals that the occurrence of an impulsive vertical shaking together with a pulse-like horizontal fault-normal seismic ground motion amplifies, on average, the displacement demand of the seismic isolator as compared to a nonpulse-like vertical excitation. In particular, this leads to a maximum average amplification of the bearing displacement equal to +14.17% (when the outliers are excluded). The highest amplification of the bearing displacement is attained at an intermediate value of the fundamental vibration period T_{1H} (i.e., $T_{1H} = 2.75$ s). This amplification reduces both at low and high fundamental vibration period values, and results approximately equal to or less than +10% (when the outliers are excluded). This is explained as follows. If the fundamental vibration period T_{1H} is low enough, then the elastomeric bearing has large stiffness in the horizontal direction, and the influence of the vertical motion on the horizontal response reduces accordingly. Conversely, if the fundamental vibration period T_{1H} is large enough, then the elastomeric bearing will experience too large horizontal displacements, and hence the premature failure regardless the vertical motion. In light of this, the condition $\Delta \to 1$ occurs more often at low and high fundamental vibration period values (even if the motivations are different), thereby reducing the displacement amplification on average.

To better figure out the relevance of a pulse-like vertical shaking, Fig. 14 also shows for the considered device that an increment of the maximum absolute displacement equal to +20% causes a contraction of the

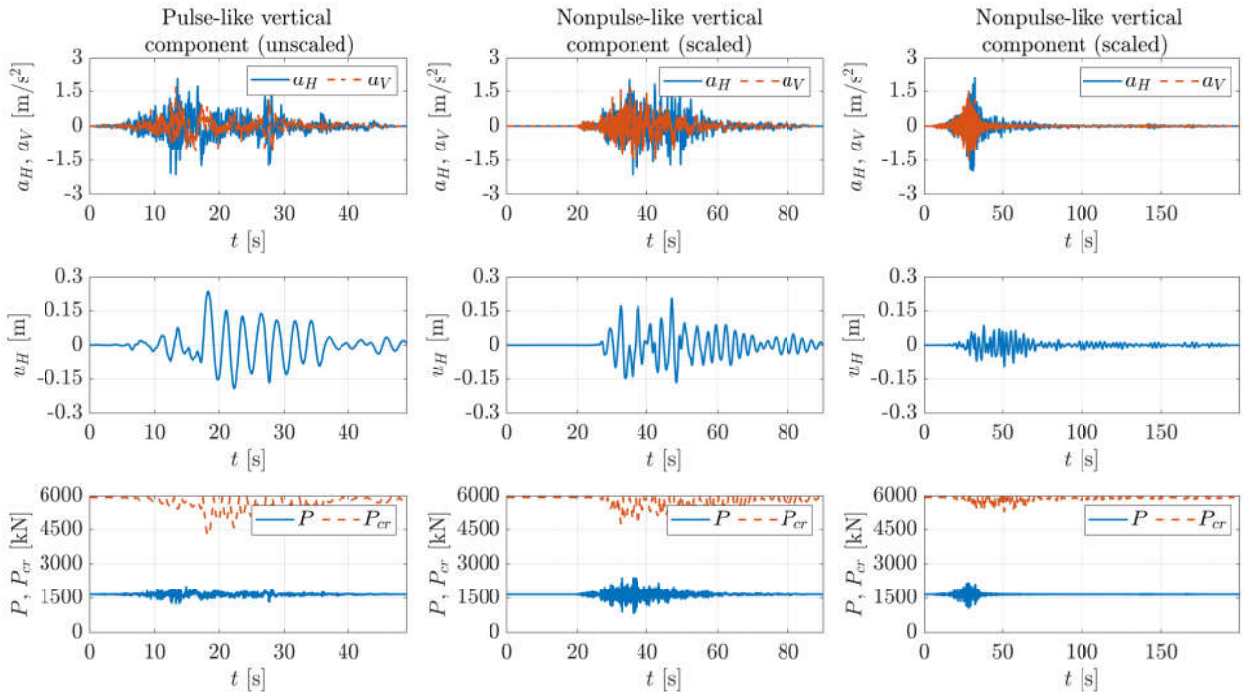

Figure 13: Analysis of the seismic bearing response subjected to pulse-like horizontal ground motion together with pulse-like (first column) and nonpulse-like (remaining columns) vertical ground motion. The seismic event with pulse-like seismic ground motion along the two directions is the 1999 Chi-Chi earthquake (TCU101 station) analyzed in Fig. 9.

reduced effective cross-section area A_r equal to -8.8% and -28.2% if the displacement demand is quarter or half the diameter, respectively. Therefore, the increment of the maximum displacement of the bearings due to a pulse-like seismic vertical ground motion as compared to a nonpulse-like vertical shaking can have significant negative impacts on the axial load capacity and the overall stability of the device. Furthermore, it is pointed out that the increment of the maximum horizontal displacement also affects the shear response, since the total shear strain of elastomeric bearings is in general the sum of shear strain due to compression, rotation and imposed lateral displacement [60].

The results for the considered device have been also confirmed for an equivalent viscous damping ratio $\xi_{1H} = 15\%$. In such case (here omitted for the sake of conciseness), the highest average amplification of the bearing displacement (without considering the outliers) reduces to $+10.36\%$ at $T_{1H} = 2.75$ s, and the scattering among the different fundamental vibration period values also decreases. Once again, this is attributable to the fact that the increment of ξ_{1H} reduces the bearing horizontal displacement, and thus mitigates the effects due to the axial component.

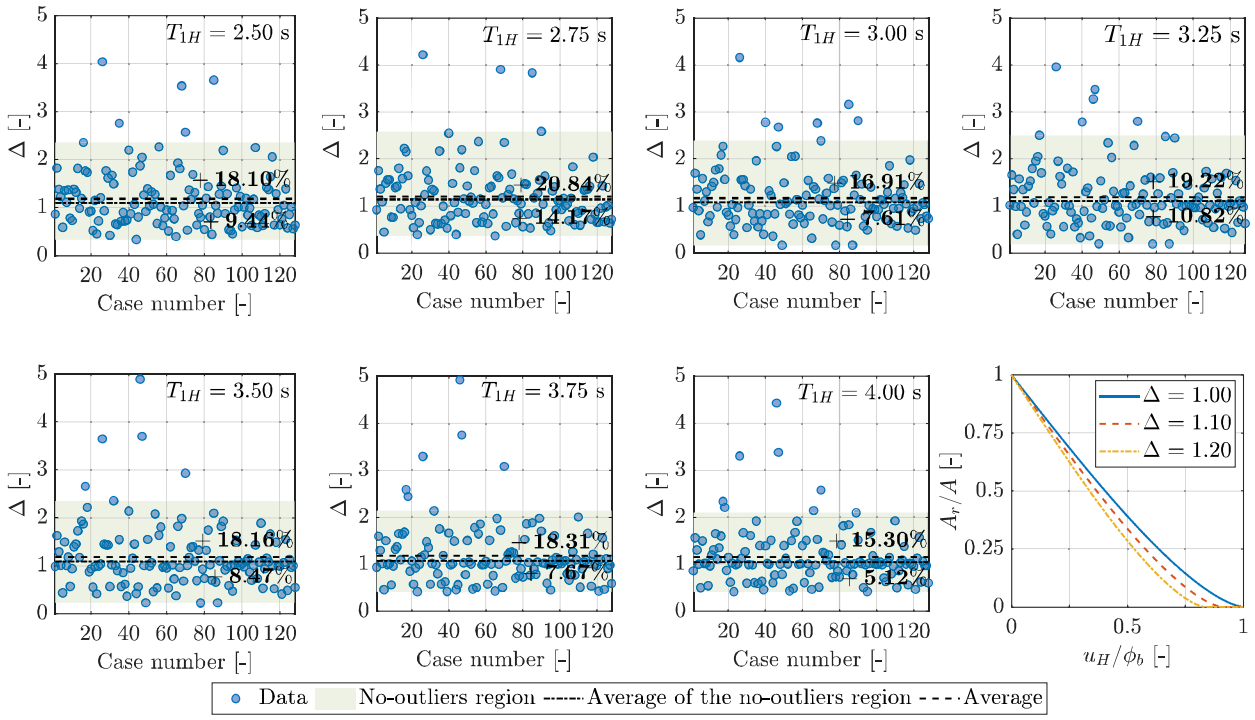

Figure 14: Ratio between the maximum bearing displacement under pulse-like ground motion along the two directions and the corresponding value under pulse-like horizontal ground motion only, together with its effect on the reduced effective cross-section area of the isolator.

Concluding remarks

The motivation of the present study was twofold. First, it was meant at providing further insights on the vertical component of near-fault pulse-like earthquakes, with focus on seismic events exhibiting an impulsive vertical component of the ground motion. Moreover, it was intended to clarify whether the occurrence of a pulse-like vertical component in such earthquakes has some effects on the response of elastomeric bearings.

As regard the first goal, the present study employed the variational mode decomposition technique to identify the impulsive waveform embedded in the horizontal fault-normal seismic ground motion component and in the vertical direction. After the characterization of the seismic records collected within the considered database, attention has been paid on the pulse period values. So doing, it is found that, if both fault-normal and vertical components embed a dominant pulse-like waveform, then the ratio of the corresponding pulse periods is well correlated with the pulse period along the fault-normal direction. Conversely, the ratio of the pulse period values is uncorrelated with respect to the pulse period along the vertical direction.

Regarding the second goal, a statistical analysis revealed that the seismic displacement of an elastomeric bearing subjected to a near-fault pulse-like ground motion can be moderately amplified, on average, if an impulsive excitation also occurs along the vertical direction. This evidence is obtained by assuming that the pulse period in the horizontal direction is similar and the peak ground accelerations in the two

components are individually the same after scaling. It is important to remark that this finding cannot be considered conclusive because of some statistical limitations. In fact, the selection strategy for the comparative evaluation of the elastomeric bearing response (i.e., sampling with replacement) is, to some extent, affected by the small database size and the quite large number of records generated from a few earthquakes, which may have introduced a statistical bias. Duration and frequency content are expected to have a limited impact on the final results as long as the impulsive component is dominated by a single pulse. However, it has been recognized that multiple pulses can occur in near-fault earthquakes, and nonpulse-like modes other than the dominant impulsive waveform can be relevant. In such cases, duration and frequency content may have some effects on the final results. Further studies should be performed in the future when the available repositories of near-fault pulse-like earthquakes will include more records.

Meanwhile, this study has pointed out that significant negative effects on axial capacity, shear strain and overall stability of elastomeric bearings can occur under horizontal pulse-like seismic ground motion if the vertical component also exhibits an impulsive waveform. This evidence may deserve a conservative reconsideration of the design guidelines for seismic isolation systems in near-fault areas. For instance, if seismic isolation systems are analyzed through nonlinear dynamic analyses paying no attention to the waveform of the vertical component (i.e., pulse- or nonpulse-like), then it would be appropriate to amplify the horizontal displacement demand according to a confidence factor in order to ensure a conservative design. This is the simplest way to cope with such issue, but a more effective and rational way passes through the definition of ad hoc selection and scaling strategies of the seismic records for nonlinear dynamic analyses of base-isolated systems in near-fault areas. Since this study has highlighted that a pulse-like vertical seismic component can have a detrimental effect on the displacement demand of elastomeric bearings employed in base-isolated buildings, future studies should investigate what happens in isolated bridges, possibly accounting for the spatial variability of the ground motion.

Acknowledgements

This work has received financial support from Sapienza University of Rome (Grant no. RG11916B4C241B32 and Grant no. RM1181640234B407).

Declaration of competing interest

The authors declare that they have no known competing financial interests or personal relationships that could have appeared to influence the work reported in this paper.

Appendix

The database of considered seismic events is provided in Table A1 (all fault-normal horizontal components of the seismic records included in this list have been classified as pulse-like).

Table A1: Full list of seismic events considered in the present study, togheter with details about the existince of pulse-like vertical component and forward directivity effect (N/A: not available).

Earthquake name (year)	Station name	M	Pulse-like vertical component	Forward directivity
Gazli (1976)	Karakyr	6.8	yes	no
Coyote Lake (1979)	Gilroy Array #6	5.74	yes	yes
Imperial Valley-06 (1979)	Brawley Airport	6.53	no	yes
Imperial Valley-06 (1979)	EC County Center FF	6.53	yes	yes
Imperial Valley-06 (1979)	EC Meloland Overpass FF	6.53	yes	yes
Imperial Valley-06 (1979)	El Centro Array #10	6.53	no	yes
Imperial Valley-06 (1979)	El Centro Array #11	6.53	yes	no
Imperial Valley-06 (1979)	El Centro Array #3	6.53	no	yes
Imperial Valley-06 (1979)	El Centro Array #4	6.53	no	yes
Imperial Valley-06 (1979)	El Centro Array #5	6.53	yes	yes
Imperial Valley-06 (1979)	El Centro Array #6	6.53	yes	yes
Imperial Valley-06 (1979)	El Centro Array #7	6.53	no	yes
Imperial Valley-06 (1979)	El Centro Array #8	6.53	yes	yes
Imperial Valley-06 (1979)	El Centro Differential Array	6.53	yes	yes
Imperial Valley-06 (1979)	Holtville Post Office	6.53	no	yes
Irpinia, Italy-01 (1980)	Sturno	6.9	yes	yes
Westmorland (1981)	Parachute Test Site	5.9	no	no
Coalinga-05 (1983)	Transmitter Hill	5.77	no	no
Coalinga-07 (1983)	Coalinga-14th & Elm (Old CHP)	5.21	no	no
Morgan Hill (1984)	Gilroy Array #6	6.19	no	yes
N. Palm Springs (1986)	North Palm Springs	6.06	no	no
San Salvador (1986)	Geotech Investig Center	5.8	no	yes
San Salvador (1986)	National Geografical Inst	5.8	no	yes
Whittier Narrows-01 (1987)	Downey - Co Maint Bldg	5.99	no	no
Whittier Narrows-01 (1987)	LB - Orange Ave	5.99	no	no
Whittier Narrows-01 (1987)	Santa Fe Springs - E.Joslin	5.99	no	no
Loma Prieta (1989)	Gilroy Array #2	6.93	yes	yes
Loma Prieta (1989)	Gilroy Array #3	6.93	no	yes
Loma Prieta (1989)	LGPC	6.93	yes	no
Loma Prieta (1989)	Saratoga - Aloha Ave	6.93	yes	yes
Cape Mendocino (1992)	Cape Mendocino	7.01	yes	no
Cape Mendocino (1992)	Petrolia	7.01	yes	yes
Landers (1992)	Lucerne	7.28	yes	yes
Landers (1992)	Yermo Fire Station	7.28	no	yes
Northridge-01 (1994)	Jensen Filter Plant	6.69	no	yes
Northridge-01 (1994)	Jensen Filter Plant Generator	6.69	no	yes
Northridge-01 (1994)	LA Dam	6.69	yes	yes
Northridge-01 (1994)	Newhall - Fire Sta	6.69	no	yes
Northridge-01 (1994)	Newhall - W Pico Canyon Rd.	6.69	yes	yes
Northridge-01 (1994)	Pacoima Dam (downstr)	6.69	yes	yes

Northridge-01 (1994)	Rinaldi Receiving Sta	6.69	no	yes
Northridge-01 (1994)	Sylmar - Converter Sta	6.69	yes	yes
Northridge-01 (1994)	Sylmar - Converter Sta East	6.69	yes	yes
Northridge-01 (1994)	Sylmar - Olive View Med FF	6.69	no	yes
Kobe (1995)	KJMA	6.9	yes	yes
Kobe (1995)	Takarazuka	6.9	yes	yes
Kobe (1995)	Takatori	6.9	no	yes
Northwest China-03 (1997)	Jiashi	6.1	yes	no
Kocaeli (1999)	Arcelik	7.51	yes	yes
Kocaeli (1999)	Duzce	7.51	no	no
Kocaeli (1999)	Gebze	7.51	no	yes
Chi-Chi (1999)	CHY006	7.62	no	yes
Chi-Chi (1999)	CHY024	7.62	yes	yes
Chi-Chi (1999)	CHY035	7.62	no	no
Chi-Chi (1999)	CHY101	7.62	no	yes
Chi-Chi (1999)	TAP003	7.62	no	no
Chi-Chi (1999)	TCU029	7.62	yes	yes
Chi-Chi (1999)	TCU031	7.62	yes	yes
Chi-Chi (1999)	TCU034	7.62	no	yes
Chi-Chi (1999)	TCU036	7.62	yes	yes
Chi-Chi (1999)	TCU038	7.62	yes	yes
Chi-Chi (1999)	TCU040	7.62	yes	yes
Chi-Chi (1999)	TCU042	7.62	yes	no
Chi-Chi (1999)	TCU046	7.62	yes	yes
Chi-Chi (1999)	TCU049	7.62	yes	yes
Chi-Chi (1999)	TCU050	7.62	yes	no
Chi-Chi (1999)	TCU052	7.62	yes	yes
Chi-Chi (1999)	TCU053	7.62	no	yes
Chi-Chi (1999)	TCU054	7.62	no	no
Chi-Chi (1999)	TCU056	7.62	yes	yes
Chi-Chi (1999)	TCU059	7.62	no	yes
Chi-Chi (1999)	TCU060	7.62	no	no
Chi-Chi (1999)	TCU063	7.62	yes	yes
Chi-Chi (1999)	TCU064	7.62	no	yes
Chi-Chi (1999)	TCU065	7.62	yes	yes
Chi-Chi (1999)	TCU068	7.62	yes	yes
Chi-Chi (1999)	TCU075	7.62	yes	yes
Chi-Chi (1999)	TCU076	7.62	no	yes
Chi-Chi (1999)	TCU082	7.62	yes	yes
Chi-Chi (1999)	TCU087	7.62	yes	yes
Chi-Chi (1999)	TCU098	7.62	no	no
Chi-Chi (1999)	TCU101	7.62	yes	yes
Chi-Chi (1999)	TCU102	7.62	yes	yes
Chi-Chi (1999)	TCU103	7.62	yes	yes
Chi-Chi (1999)	TCU104	7.62	no	yes
Chi-Chi (1999)	TCU106	7.62	no	no
Chi-Chi (1999)	TCU111	7.62	no	no
Chi-Chi (1999)	TCU116	7.62	no	no
Chi-Chi (1999)	TCU128	7.62	yes	yes
Chi-Chi (1999)	TCU136	7.62	yes	yes
Chi-Chi (1999)	CHY024	6.2	yes	no
Chi-Chi (1999)	CHY080	6.2	yes	no

Chi-Chi (1999)	TCU076	6.2	yes	no
Duzce (1999)	Duzce	7.14	yes	no
Yountville (2000)	Napa Fire Station #3	5	no	no
Bam (2003)	BAM	6.6	no	yes
Parkfield (2004)	Cholame 1E	6	no	yes
Parkfield (2004)	Cholame 2W	6	yes	yes
Parkfield (2004)	Cholame 4W	6	yes	yes
Parkfield (2004)	Fault Zone 1 (COW)	6	no	yes
Parkfield (2004)	Eades	6	no	yes
Parkfield (2004)	Fault Zone 12 (PRK)	6	no	yes
Parkfield (2004)	Stone Corral (SC1)	6	no	yes
Parkfield (2004)	Fault Zone 14	6	no	no
Niigata (2004)	NIGH11	6.63	no	yes
Montenegro (1979)	Bar-Skupstina Opstine	7.1	no	yes
L'Aquila (2009)	L'Aquila - AQG	6.3	no	no
L'Aquila (2009)	L'Aquila - AQV	6.3	no	yes
Chuetsu-oki (2007)	Kashiwazaki City Center	6.8	no	no
Chuetsu-oki (2007)	Kariwa	6.8	yes	no
Chuetsu-oki (2007)	Service Hall: 2.4 m depth	6.8	no	no
Iwate (2008)	Machimukai Town	6.9	no	no
El Mayor-Cucapah (2010)	Tamaulipas	7.2	no	no
Joshua Tree (1992)	Indio - Jackson Road	6.1	yes	no
Darfield (2010)	DSLC	7	no	yes
Darfield (2010)	GDLC	7	no	yes
Darfield (2010)	LINC	7	yes	yes
Darfield (2010)	NNBS	7	yes	yes
Darfield (2010)	ROLC	7	no	yes
Darfield (2010)	SHLC	7	yes	yes
Darfield (2010)	SMTC	7	no	yes
Christchurch (2011)	CCCC	6.2	no	no
Christchurch (2011)	CMHS	6.2	no	no
Christchurch (2011)	REHS	6.2	no	yes
Christchurch (2011)	SHLC	6.2	yes	no
Christchurch (2011)	LPCC	6.2	yes	no
El Mayor-Cucapah (2010)	El Centro Array #12	7.2	no	yes
El Mayor-Cucapah (2010)	Westside Elementary School	7.2	no	yes
Lorca (2011)	N/A	5.2	yes	yes
Ölfus (2008)	Hveragerdi-Retirement House	6.3	yes	yes
Ölfus (2008)	Selfoss-City Hall	6.3	yes	yes
Central Italy (2016)	Amatrice	6	yes	yes
Central Italy (2016)	Campi	5.9	no	no

References

[1] Babak Alavi and Helmut Krawinkler. Behavior of moment-resisting frame structures subjected to near-fault ground motions. *Earthquake engineering & structural dynamics*, 33(6):687–706, 2004.

[2] G. G. Amiri and S. A. Moghaddam. Extraction of forward-directivity velocity pulses using S-Transform-based signal decomposition technique. *Bulletin of Earthquake Engineering*, 12(4):1583–1614, 2014.

[3] J. W. Baker. Quantitative classification of near-fault ground motions using wavelet analysis. *Bulletin of the Seismological Society of America*, 97(5):1486–1501, 2007.

[4] M Bhandari, SD Bharti, MK Shrimali, and TK Datta. The numerical study of base-isolated buildings under near-field and far-field earthquakes. *Journal of Earthquake Engineering*, 22(6):989–1007, 2018.

[5] Z. Chang, X. Sun, C. Zhai, J. X. Zhao, and L. Xie. An improved energy-based approach for selecting pulse-like ground motions. *Earthquake Engineering & Structural Dynamics*, 45(14):2405–2411, 2016.

[6] Mayssa Dabaghi and Armen Der Kiureghian. Simulation of orthogonal horizontal components of near-fault ground motion for specified earthquake source and site characteristics. *Earthquake Engineering & Structural Dynamics*, 47(6):1369–1393, 2018.

[7] Aydin Daei, Mehdi Poursha, and Mohamad Zarrin. Seismic performance evaluation of code-compliant rc moment-resisting frame buildings subjected to near-fault pulse-like and non-pulse-like ground motions. *Journal of Earthquake Engineering*, pages 1–28, 2021.

[8] Nhan D Dao, Hieu Nguyen-Van, Tuan HA Nguyen, and Ai B Chung. A new statistical equation for predicting nonlinear time history displacement of seismic isolation systems. 24:177–190, 2020.

[9] A Di Matteo, C Masnata, and A Pirrotta. Simplified analytical solution for the optimal design of tuned mass damper inerter for base isolated structures. *Mechanical Systems and Signal Processing*, 134:106337, 2019.

[10] Ahmet Anıl Dindar, Cem Yalçın, Ercan Yüksel, Hasan Özkaynak, and Oral Büyüköztürk. Development of earthquake energy demand spectra. *Earthquake Spectra*, 31(3):1667–1689, 2015.

[11] J Donaire-Avila, A Benavent-Climent, A Escobedo, and E Oliver-Saiz. Damage assessment on building structures subjected to the recent near-fault earthquake in Lorca (Spain). In *Proceedings of the 15th World Conference on Earthquake Engineering*, 2012.

[12] J Donaire-Ávila, F Mollaioli, A Lucchini, and A Benavent-Climent. Intensity measures for the seismic response prediction of mid-rise buildings with hysteretic dampers. *Engineering Structures*, 102:278–295, 2015.

[13] K. Dragomiretskiy and D. Zosso. Variational mode decomposition. *IEEE Transactions on Signal Processing*, 62(3): 531–544, 2014.

[14] Amr S Elnashai and Luigi Di Sarno. *Fundamentals of earthquake engineering*. Wiley New York, 2008.

[15] Deniz Ertuncay and Giovanni Costa. Determination of near-fault impulsive signals with multivariate naïve bayes method. *Natural Hazards*, pages 1–18, 2021.

[16] Jun Feng, Boming Zhao, and Tianci Zhao. Quantitative identification of near-fault pulse-like ground motions based on variational mode decomposition technique. *Soil Dynamics and Earthquake Engineering*, 151:107009, 2021.

[17] Massimiliano Ferraioli and Alberto Mandara. Base isolation for seismic retrofitting of a multiple building structure: evaluation of equivalent linearization method. *Mathematical Problems in Engineering*, 2016, 2016.

[18] Mohsen Gerami and Davood Abdollahzadeh. Vulnerability of steel moment-resisting frames under effects of forward directivity. *The Structural Design of Tall and Special Buildings*, 24(2):97–122, 2015.

[19] SF Ghahari, HR Moradnejad, MS Rouhanimanesh, and A Sarvghad-Moghadam. Studying higher mode effects on the performance of nonlinear static analysis methods considering near-fault effects. *KSCE Journal of Civil Engineering*, 17 (2):426–437, 2013.

[20] Ioannis Gidaris, Alexandros A Taflanidis, and George P Mavroeidis. Kriging metamodeling in seismic risk assessment based on stochastic ground motion models. *Earthquake Engineering & Structural Dynamics*, 44(14):2377–2399, 2015.

[21] Ioannis Gidaris, Alexandros A Taflanidis, Diego Lopez-Garcia, and George P Mavroeidis. Multi-objective risk-informed design of floor isolation systems. *Earthquake Engineering & Structural Dynamics*, 45(8):1293–1313, 2016.

[22] Ahed Habib, Ausamah AL Houri, and Umut Yildirim. Comparative study of base-isolated irregular rc structures subjected to pulse-like ground motions with low and high pga/pgv ratios. *Structures*, 31:1053–1071, 2021.

[23] John F Hall, Thomas H Heaton, Marvin W Halling, and David J Wald. Near-source ground motion and its effects on flexible buildings. *Earthquake spectra*, 11(4):569–605, 1995.

[24] Benedikt Halldórsson, George P Mavroeidis, and Apostolos S Papageorgiou. Near-fault and far-field strong ground-motion simulation for earthquake engineering applications using the specific barrier model. *Journal of Structural Engineering*, 137(3):433–444, 2011.

[25] RS Jangid and JM Kelly. Base isolation for near-fault motions. *Earthquake engineering & structural dynamics*, 30(5): 691–707, 2001.

[26] Gaofeng Jia, Ioannis Gidaris, Alexandros A Taflanidis, and George P Mavroeidis. Reliability-based assessment/design of floor isolation systems. *Engineering Structures*, 78:41–56, 2014.

[27] Vishal Kamble, Shiv Dayal Bharti, Mahendra Kumar Shrimali, and Tushar Kanti Datta. Control of secondary systems response in a base-isolated building under tridirectional ground motion. *Practice Periodical on Structural Design and Construction*, 27(1):04021060, 2022.

[28] Ali Khansefid. Pulse-like ground motions: Statistical characteristics, and gmpe development for the iranian plateau. *Soil Dynamics and Earthquake Engineering*, 134:106164, 2020.

[29] M Kuleli and AS Elnashai. Cable-stayed bridges subjected to near-fault vertical motion. In *4th International Conference on Computational Methods in Structural Dynamics and Earthquake Engineering, COMPDYN 2013*, 2013.

[30] Jeevan A Kulkarni and RS Jangid. Rigid body response of base-isolated structures. *Journal of structural control*, 9(3): 171–188, 2002.

[31] Cuihua Li, Zhanxuan Zuo, Sashi Kunnath, and Linli Chen. Orientation of the strongest velocity pulses and the maximum structural response to pulse-like ground motions. *Soil Dynamics and Earthquake Engineering*, 136:106240, 2020.

[32] Wen-I Liao, Chin-Hsiung Loh, and Shiuan Wan. Earthquake responses of rc moment frames subjected to near-fault ground motions. *The Structural Design of Tall Buildings*, 10(3):219–229, 2001.

[33] Tao Liu, Tobia Zordan, Bruno Briseghella, and Qilin Zhang. An improved equivalent linear model of seismic isolation system with bilinear behavior. *Engineering Structures*, 61:113–126, 2014.

[34] Nicos Makris. Rigidity–plasticity–viscosity: Can electrorheological dampers protect base-isolated structures from near-source ground motions? *Earthquake Engineering & Structural Dynamics*, 26(5):571–591, 1997.

[35] Iman Mansouri, Shahrokh Shahbazi, Jong Wan Hu, and Salar Arian Moghaddam. Effects of pulse-like nature of forward directivity ground motions on the seismic behavior of steel moment frames. *Earthq. Struct*, 17:1–15, 2019.

[36] Emiliano Matta. Effectiveness of tuned mass dampers against ground motion pulses. *Journal of Structural Engineering*, 139(2):188–198, 2013.

[37] G. P Mavroeidis and A. S. Papageorgiou. A mathematical representation of near-fault ground motions. *Bulletin of the Seismological Society of America*, 93(3):1099–1131, 2003.

[38] Fabio Mazza. Seismic demand of base-isolated irregular structures subjected to pulse-type earthquakes. *Soil Dynamics and Earthquake Engineering*, 108:111–129, 2018.

[39] Fabio Mazza and Rodolfo Labernarda. Structural and non-structural intensity measures for the assessment of base-isolated structures subjected to pulse-like near-fault earthquakes. *Soil Dynamics and Earthquake Engineering*, 96:115–127, 2017.

[40] Fabio Mazza and Mirko Mazza. Influence of elastomeric bearings in tension on the seismic performance of base-isolated rc buildings. *Applied Sciences*, 11(1):82, 2021.

[41] Fabio Mazza and Mirko Mazza. Nonlinear modelling of hdrbs in the seismic analysis of retrofitted and new base-isolated rc buildings. *Structures*, 33:4148–4161, 2021.

[42] Fabio Mazza and Alfonso Vulcano. Effects of near-fault ground motions on the nonlinear dynamic response of base-isolated rc framed buildings. *Earthquake Engineering & Structural Dynamics*, 41(2):211–232, 2012.

[43] C. Menun and Q. Fu. An analytical model for near-fault ground motions and the response of SDOF systems. In *Proceedings*

of the 7th US National Conference on Earthquake Engineering, 2002.

[44] P. Mimoglou, I. N. Psycharis, and I. M. Taflampas. *Determination of the parameters of the directivity pulse embedded in near-fault ground motions and its effect on structural response*, pages 27–48. Springer International Publishing, 2017.

[45] G Minasidis, GD Hatzigeorgiou, and DE Beskos. Ssi in steel frames subjected to near-fault earthquakes. *Soil Dynamics and Earthquake Engineering*, 66:56–68, 2014.

[46] Sebastián Miranda, Eduardo Miranda, and Juan Carlos de la Llera. A simplified and versatile element model for elastomeric seismic isolation bearings. *Earthquake Spectra*, page 87552930211030939, 2021.

[47] Fabrizio Mollaioli and Anna Bosi. Wavelet analysis for the characterization of forward-directivity pulse-like ground motions on energy basis. *Meccanica*, 47(1):203–219, 2012.

[48] Fabrizio Mollaioli, Andrea Lucchini, Yin Cheng, and Giorgio Monti. Intensity measures for the seismic response prediction of base-isolated buildings. *Bulletin of Earthquake Engineering*, 11(5):1841–1866, 2013.

[49] Abbas Moustafa and Izuru Takewaki. Deterministic and probabilistic representation of near-field pulse-like ground motion. *Soil Dynamics and Earthquake Engineering*, 30(5):412–422, 2010.

[50] Taha Nazarnezhad and Hosein Naderpour. Probabilistic damage evaluation of base-isolated reinforced concrete structures under near-fault pulse-like bidirectional seismic excitations. *Structures*, 32:1156–1170, 2021.

[51] Giuseppe Quaranta and Fabrizio Mollaioli. Analysis of near-fault pulse-like seismic signals through variational mode decomposition technique. *Engineering Structures*, 193:121–135, 2019.

[52] Giuseppe Quaranta, Giuseppe Carlo Marano, Rita Greco, and Giorgio Monti. Parametric identification of seismic isolators using differential evolution and particle swarm optimization. *Applied Soft Computing*, 22:458–464, 2014.

[53] Giuseppe Quaranta, Fabrizio Mollaioli, and Giorgio Monti. Effectiveness of design procedures for linear tmd installed on inelastic structures under pulse-like ground motion. *Earthquakes and Structures*, 10(1):239–260, 2016.

[54] Giuseppe Quaranta, Walter Lacarbonara, and Sami F Masri. A review on computational intelligence for identification of nonlinear dynamical systems. *Nonlinear Dynamics*, 99(2):1709–1761, 2020.

[55] Panayiotis C Roussis, Michael C Constantinou, Mustafa Erdik, Eser Durukal, and Murat Dicleli. Assessment of performance of seismic isolation system of bolu viaduct. *Journal of Bridge Engineering*, 8(4):182–190, 2003.

[56] Arijit Saha and Sudib Kumar Mishra. Amplification of seismic demands in inter-storey-isolated buildings subjected to near fault pulse type ground motions. *Soil Dynamics and Earthquake Engineering*, 147:106771, 2021.

[57] Jonathan Salvi, Egidio Rizzi, Emiliano Rustighi, and Neil S Ferguson. Optimum tuning of passive tuned mass dampers for the mitigation of pulse-like responses. *Journal of Vibration and Acoustics*, 140(6):061014, 2018.

[58] Farshad Taiyari, Antonio Formisano, and Federico M Mazzolani. Seismic behaviour assessment of steel moment resisting frames under near-field earthquakes. *International Journal of Steel Structures*, 19(5):1421–1430, 2019.

[59] Alper Ucak, George P Mavroeidis, and Panos Tsopelas. Behavior of a seismically isolated bridge crossing a fault rupture zone. *Soil Dynamics and Earthquake Engineering*, 57:164–178, 2014.

[60] Niel C Van Engelen, Dimitrios Konstantinidis, and Michael J Tait. Shear strain demands in elastomeric bearings subjected to rotation. *Journal of Engineering Mechanics*, 143(4):04017005, 2017.

[61] Zhou Xu and Anil Agrawal. Decomposition and effects of pulse components in near-field ground motions. *Journal of Structural Engineering*, 136(6):690–699, 2010.

[62] Saman Yaghmaei-Sabegh, Ebrahim Jafari-Koucheh, and Mehdi Ebrahimi-Aghabagher. Estimating the seismic response of nonlinear structures equipped with nonlinear viscous damper subjected to pulse-like ground records. *Structures*, 28: 1915–1923, 2020.

[63] Fujian Yang, Guoxin Wang, and Yang Ding. Damage demands evaluation of reinforced concrete frame structure subjected to near-fault seismic sequences. *Natural Hazards*, 97(2):841–860, 2019.

[64] Changhai Zhai, Zhiwang Chang, Shuang Li, ZhiQiang Chen, and Lili Xie. Quantitative identification of near-fault pulse-

like ground motions based on energy. *Bulletin of the Seismological Society of America*, 103(5):2591–2603, 2013.